AIAA JOURNAL
Vol. 54, No. 7, July 2016

Computation of Supersonic Branching Flow with Aerosol Particle Separation

Bofeng Bai* and Xing Li†
Xi'an Jiaotong University, 710049 Xi'an, People's Republic of China
and
Shuiqing Li‡
Tsinghua University, 100084 Beijing, People's Republic of China

DOI: 10.2514/1.J054533

Supersonic branching flows are commonly found in industrial processes like the supersonic aerosol particle separation process and the supersonic inlet of combined aeroengines. In this research, we carry out a numerical study on the supersonic branching flow to reveal its features and its effects on aerosol particle separation. It is found that there are four flow regimes and a critical state in the supersonic branching flow in terms of the shock wave positions, which are determined by the backpressures of the two outlets. The gas flow rate ratio and the particle separation ratio are closely related to the flow regimes. There is a steady working zone where the gas flow rate ratio and the particle separation ratio maintain as constant as the two backpressures vary. In swirling flows, there is a drift of the critical state. In the range of particle sizes studied here, the particle motion is not sensitive to the variations of the particle size in the absence of swirl, but it is not the case for swirling flows. Finally, some features of the steady working zone are discussed. This work is a preliminary research into supersonic branching flow and provides a foundation for the design of relevant devices.

Nomenclature

a	=	radius of particle, m
C_B	=	circumference at point B, m
C_D	=	drag coefficient
c_p	=	specific heat capacity, J · kg^{-1} · K^{-1}
F_B	=	Brownian force on a particle, N
F_D	=	drag force on a particle, N
F_S	=	Saffman lift force on a particle, N
F_T	=	thermophoretic force on a particle, N
f_T	=	dimensionless thermophoretic force
Kn	=	Knudsen number
M	=	Mach number
M_p	=	particle Mach number
m_p	=	mass of a particle, kg
$\dot{m}_{\text{out}}$	=	actual gas flow rate of the outer channel, kg · s^{-1}
$\dot{m}'_{\text{out}}$	=	gas flow rate of the outer channel on frictionless condition, kg · s^{-1}
$\dot{m}_{\text{total}}$	=	actual total gas flow rate, kg · s^{-1}
$\dot{m}'_{\text{total}}$	=	gas total flow rate on frictionless condition, kg · s^{-1}
Re	=	Reynolds number
Re_p	=	particle Reynolds number
Re_x	=	Reynolds number with characteristic length scale x
St	=	Stokes number
T	=	temperature of the gas, K
T_∞	=	temperature of the gas at the edge of the boundary layer, K
V	=	velocity of the gas, m · s^{-1}
V_B	=	velocity of the gas at the edge of the boundary layer at point B, m · s^{-1}
V_∞	=	velocity of the gas at the edge of the boundary layer, m · s^{-1}
ΔV	=	relative velocity between the particle and the fluid, m · s^{-1}
$\Delta\dot{m}$	=	loss of the gas flow rate in the presence of friction, kg · s^{-1}
δ	=	thickness of the boundary layer, m
δ^*	=	displacement thickness of the boundary layer, m
ζ_i	=	zero-mean unit-variance-independent Gaussian random number
η	=	actual gas flow rate ratio
μ	=	dynamic viscosity of fluid, Pa · s
ν	=	kinematic viscosity of fluid, m^2 · s
ρ	=	density of the gas, kg · m^{-3}
ρ_B	=	density of the gas at the edge of the boundary layer at point B, kg · m^{-3}
ρ_∞	=	density of the gas at the edge of the boundary layer, kg · m^{-3}

Received 7 June 2015; revision received 16 November 2015; accepted for publication 27 January 2016; published online 4 May 2016.

*Professor, State Key Laboratory of Multiphase Flow in Power Engineering, Shaanxi; bfbai@mail.xjtu.edu.cn (Corresponding Author).

†Ph.D. Student, State Key Laboratory of Multiphase Flow in Power Engineering, Shaanxi; lx20032006@stu.xjtu.edu.cn.

‡Professor, Key Laboratory for Thermal Science and Power Engineering of Ministry of Education, Department of Thermal Engineering; lishuiqing@mail.tsinghua.edu.cn.

I. Introduction

THE supersonic branching flow is wall-bounded flow consisting of the main pipe flow and two branching flows. It is widely present in industrial processes like combined aeroengines and supersonic separation devices. The inlet of the combined turbo/ramjet aeroengine has two branches leading the air to the turbojet and the ramjet. The transition between the turbojet mode and the ramjet mode, which is vital for the performance of the engine, is closely related to the branching flow. In the supersonic separation process, particles (or droplets) are separated in supersonic swirling flow where supersonic branching flow occurs. When the particles are introduced into the flow, the two-phase supersonic branching flow is a complex process involving many fundamental issues like the shock wave motion in the tube, particle motion in wall-bounded turbulent flows, the effects of the shock wave on particle motion, and even the particle motion in swirling flows.

Generally speaking, the shock wave in a de Laval nozzle moves as the ratio of the outlet pressure to the inlet pressure changes. A similar phenomenon occurs in the supersonic branching flow. However, the shock wave position is affected by the two outlets in the branching flow. In addition, the study on the flow rate distribution in the two branches has practical significance since, in real applications, the flow rate ratio is an important parameter.

The motion and dispersion of aerosol particles in wall-bounded turbulent flows are essential in the supersonic branching flow. Direct numerical simulation (DNS) works reveal that coherent structures play a very important role in the particle entrainment and deposition process [1–3]. Near-wall sweep and ejection events of the fluid enable the particles to move toward and away from the wall, resulting in a preferential accumulation of particles below the low-speed streaks in the viscous sublayer [4]. The particle inertia is also an important factor. Particles with larger inertia are less likely to follow the carrier fluid. It is found that, in isotropic turbulence, the particles with $St \approx 1$ show the most obvious preferential concentration. But, in wall-bounded turbulence, investigation shows that maximum segregation occurs at $St \approx 25$ [5]. However, at the supersonic speed, DNS on full-scale particle-laden turbulence is impractical. Many alternatives are available, including large-eddy simulation (LES). But, still, the resource the LES requires is still large.

A shock wave in the supersonic branching flow may influence the motion of the particles. If the shock emerges in front of the branching point, it may greatly affect the separation efficiency. The direction of the particles changes when the particles move through an oblique shock wave, but not if the shock is normal. And, if the droplets pass the shock wave, they may break up when they are large enough [6,7] or evaporate when their size is in micrometers [8]. Meanwhile, the shock wave may cause boundary-layer separation, in which case the turbulent boundary-layer flow structure changes and the particle dispersion may be seriously affected. In some cases, the presence of particles also affects the shock wave [9].

In a previous paper, Li and Bai studied the particle motion in supersonic laminar boundary layers [10]. The objective of this paper is to investigate the important features that influence the aerosol particle motion in supersonic branching flow, especially the features of the supersonic branching flow and particle motion in the turbulent boundary layer near the wall. In this paper, a two-dimensional model is built to investigate the aerosol particle separation in the supersonic branching flow. The particles are tracked in a Lagrangian way, and the flowfield is calculated in an Eulerian grid. First, we investigate the nonswirl two-phase flowfield and the trends of both the gas flow rate ratio and the particle flow rate ratio. Then, we examine the flowfield in the presence of swirl and the influence of the particle diameter. Finally, we focus our discussion on one of the four regimes in supersonic branching flows.

II. Problem Description

The geometrical structure of the branching flow channel is shown in Fig. 1. The main channel, outer channel, and inner channel make up the main part of the branching structure. To establish a supersonic flowfield in the main channel, the gas is accelerated to Mach 1 at point A (i.e., the throat) by the accelerating part, which is a converging channel. The cross-sectional radius at point A is 4.78 mm. The accelerating part is an annular pipe, and it is used to create a highly swirling flow (see Sec. V.C). The annular pipe changes to a circular one at point A. The main channel is slightly diverging, accelerating the gas to about Mach 1.55 at point B, i.e., the branching point. Then, the flow is split into two streams: one into the inner channel, and the other into the outer channel. The cross-sectional radii of the inner channel and the main channel at point B are 4.6 and 5.45 mm, respectively. In our study, the total pressure and total temperature are 0.7 MPa and 300 K, respectively.

The particles are injected from the throat surface at point A, and they are uniformly distributed along the surface. The initial velocity of the particle is the same as the velocity of the surrounding gas. When the particles are injected into the channel, some will enter the outer channel. As the outer channel is adjacent to the main channel wall and the thickness of the boundary layer in the main channel is close to the width of the outer channel, the number of the particles entering the outer channel is seriously affected by the boundary layer. For the dispersed phase, as the flow is supersonic and the velocity and temperature gradient are large under some circumstances, the drag force, lift force, and thermophoretic force on the particles are considered. Because the particles are of the micrometer scale, the Brownian force is also taken into consideration. In our study, the particle-to-gas density ratio is large enough, so unsteady forces including Basset force and added mass force are neglected. This thinking was justified by Bagchi and Balachandar [11] and Ling et al. [12], who concluded that the net effects of the unsteady forces could not be neglected when the particle-to-gas density ratio was small, and their effects tended to decrease as the density ratio increased and the initial particle Reynolds number decreased. Owing to the dilute dispersion of the particles, the particle–particle interaction was negligible. To calculate the number of the separated particles, we assume that all the particles reach the outlet, which means the particles reflect from the wall once they touch the wall, and they do not deposit. The particles are regarded as spherical and monodispersed. In this work, the heat and mass transfer between the dispersed phase and the continuous phase and the effect of the particles on the carrier fluid are not taken into account.

III. Methodology

Many methods for simulating particle flows are available [13,14], and we prefer the Eulerian–Lagrangian method in our study. Our model is established on the basis of the FLUENT code. As the branching flow channel is axisymmetric, the axisymmetric formulation is applied. This formulation works well for nonswirling flows. For swirling flows, the drawback of the axisymmetric formulation is that the three-dimensional flowfield inside the vortex breakdown zone cannot be accurately predicted. Outside the breakdown zone, the swirling flowfield can be fairly simulated. The breakdown point can also be precisely predicted [15]. It is shown in Sec. V.C that, in this research, the three-dimensional flow features inside the breakdown zone are not important for the particle separation. Therefore, the axisymmetric formulation is suitable for our research, despite its weakness in predicting the flow inside the breakdown zone.

The supersonic flowfield is modeled with the Eulerian method, and the particles are tracked with the Lagrangian method. The Reynolds stress turbulence model is applied to calculate the flowfield. As the gas in this case cannot be regarded as ideal, the Redlich–Kwong equation of state is applied. Because the particle–fluid flow is one-way coupled, there is no source term in the continuous equations.

For the dispersed phase, the motion of particles is governed by Newton's second law of motion:

$$m_p \frac{\mathrm{d}^2 x}{\mathrm{d}t^2} = F_D + F_T + F_S + F_B \tag{1}$$

where m_p is the particle mass; F_D is the drag force; F_T is the thermophoretic force; F_S is the Saffman lift force; and F_B is the Brownian force.

The force models are important in deciding the particle motion. Since the flow is compressible and the particle is small, the effects of

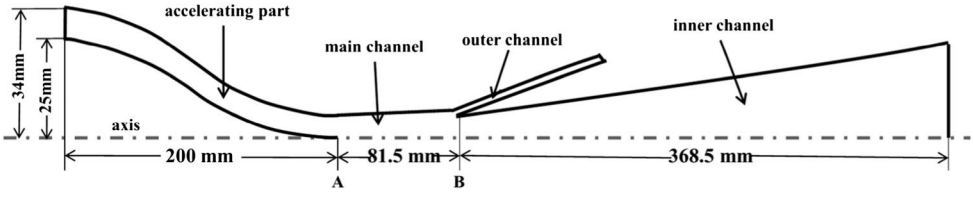

Fig. 1 Schematic of supersonic branching flow.

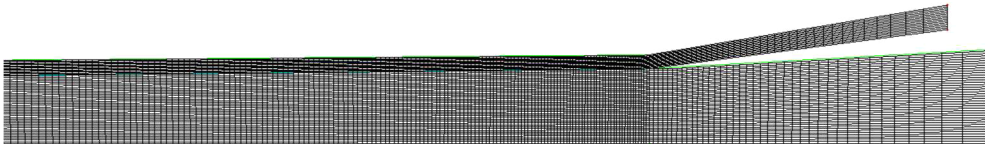

Fig. 2 Mesh near the branching point.

compressibility and rarefaction have to be taken into account. Loth [16] elaborately analyzed their effects on the drag of spherical particles and proposed drag force models for the rarefaction-dominated regime when $Re_p \leqslant 45$ and the compressibility-dominated regime when $\mathrm{Re}_p > 45$. This model is proved to be in good accordance with the experimental results [16], thus, it is applied to calculate the drag force on particles in our research. The expressions involved are as follows:

$$C_D = \frac{C_{D,Kn,Re}}{1 + M_p^4} + \frac{M_p^4 C_{D,fm,Re}}{1 + M_p^4} \quad \text{for} \quad Re \leq 45 \tag{2}$$

$$C_D = \frac{24}{Re_p}[1 + 0.15Re_p^{0.687}]H_M + \frac{0.42C_M}{1 + (42,500G_M/Re_p^{1.16})} \quad \text{for} \quad Re_p > 45 \tag{3}$$

where $C_{D,Kn,Re}$, $C_{D,fm,Re}$, H_M, C_M, and G_M are intermediate parameters for calculating C_D. The range of Knudsen numbers in our research is wide, from nearly 0.005 to 1.0. For the thermophoretic force model in the transitional regime, Yamamato and Ishihara [17] proposed a relatively more accurate expression as follows by solving the Boltzmann equation numerically, and it is applicable for our case:

$$f_T = \frac{16\pi}{5}\left[A_w H_o - A_o\left(H_w + \frac{5\sqrt{\pi}}{4}Kn\hat{k}\right)\right]\left(H_w + \frac{5\sqrt{\pi}}{4}Kn\hat{k}\right)^{-1} \tag{4}$$

where A_w, A_o, H_w, and H_o are functions of the Knudsen number, and $\hat{k}$ is the ratio of thermal conductivity of the particle to that of the gas.

In shear flows, the particle experiences a lift force perpendicular to its moving direction. Saffman [18] proposed its expression $F_S = 6.46\mu a^2 \Delta V \nu^{-1/2}(\mathrm{d}V/\mathrm{d}y)^{1/2}$, and it has been widely used in studies. Dandy and Dwyer [19], McLaughlin [20], Mei [21], Kurose and Komori [22], and Bagchi and Balachandar [23] proposed different expressions of the lift force model, but Saffman's [18] meets our accuracy requirement and is more manageable; thus, it is adopted in our research. The Brownian force is modeled as a Gaussian white noise random process:

$$F_{Bi} = \zeta_i \sqrt{\frac{\pi S_o}{\Delta t}} \tag{5}$$

Turbulence is modeled in Reynolds-averaged Navier–Stokes equations and, accordingly, the particle motion and dispersion caused by turbulence are modeled. The random walking model and the particle cloud model are generally used in the particle motion model. In our research, the cloud model is adopted.

The mesh we use in this research is structured but not uniform. To accurately capture the flow in the near-wall region, the grid near the wall is refined. In addition, the particle separation is also one of our focuses, so the grid near the branching point is also refined, as shown in Fig. 2.

IV. Validation

To check the accuracy of the simulation, a grid-dependence check is operated. The meshes with 6000, 12,000, 26,000, and 46,000 elements are investigated. We refine the mesh as a whole, which means only the element number increases but the local refinement

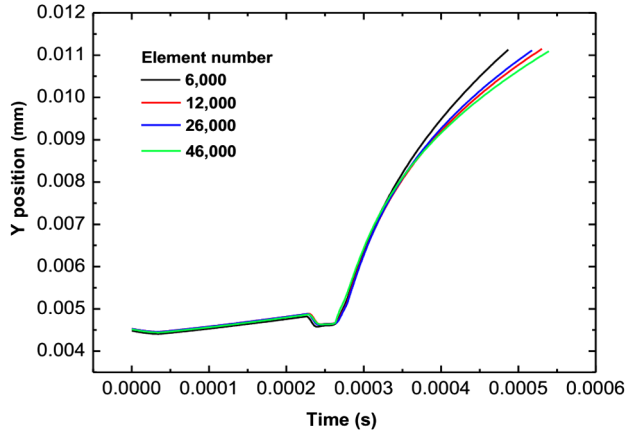

Fig. 3 Grid-dependence check.

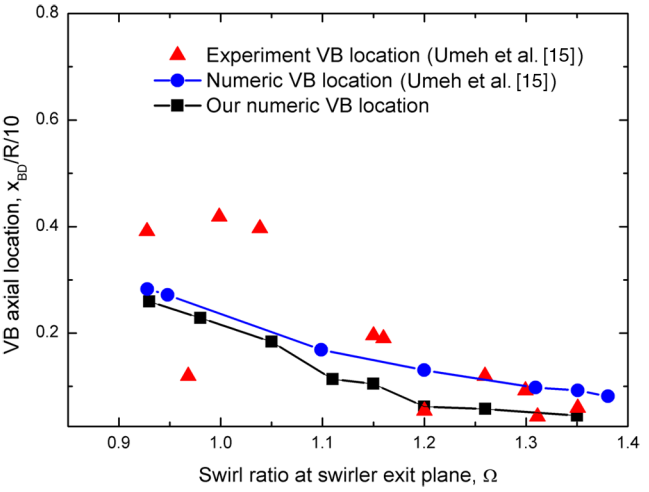

Fig. 4 Comparison of vortex breakdown (VB) points.

method holds for all the meshes. The particle mean trajectories injected from the same initial position are compared. Figure 3 shows that the simulations with meshes of more than 26,000 elements produce almost the same result. So, the mesh with 26,000 is preferable in the simulation.

We have also examined the vortex breakdown point in compressible swirling flows to check the validity of the single-phase model. The experiment setup is demonstrated in [15]. We build geometry that is the same as the one in the numerical investigation of Umeh et al. [15], and we simulate the flowfield using our single-phase model. The element number of the grid we use is a little larger than the one used by Umeh et al. [15]. In Fig. 4, the scattered experimental vortex breakdown points indicate the unsteady nature of the flow. Because of the unsteadiness, the vortex breakdown point moves back and forth and is difficult to locate. In our simulation, we also noticed this unsteady nature. We take the average position of the fluctuating vortex breakdown point as our numeric vortex breakdown location. It turns out that the vortex breakdown points predicted by our model agree well with the experimental ones, although they are slightly nearer to the dump plane (the axial location of the dump plane is 0.0) than the ones predicted by the numerical model of Umeh et al. [15].

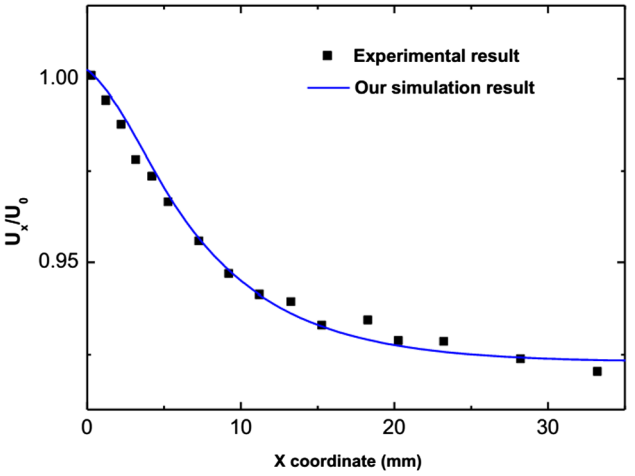

Fig. 5 Validation of the model.

Another validation is done by comparing the simulation result with the experimental result of the particles' x-directional velocity distribution after the oblique shock wave given by Tedeschi et atl. [24]. The case of the incense smoke particles with diameters of 1.4 μm is studied in our validation. From Fig. 5, we can see that the simulation agrees with the experiment.

V. Results

A. Four Flow Regimes in Supersonic Branching Flow

To investigate the properties of the particle motion in the branching flow, the single-phase gas flowfield has to be studied first. The flow in this part is nonswirling. Among all the characteristics of the gas flow, the one that interests us most is the change of the shock wave position as the backpressures of the two outlets vary.

According to the aerodynamics in a de Laval nozzle, the backpressure has a great effect on the shock position. The supersonic flow changes abruptly into subsonic when crossing the shock wave. As the backpressure increases, the shock position moves upstream. However, some differences exist in the supersonic branching flow. As we can see in Fig. 6c, there are shock waves in both of the branches when their backpressures are relatively low. As the backpressures increase gradually when the total pressure is kept constant at 0.7 MPa, the shock waves move upstream. The two backpressures can be increased high enough for both of the shock waves to stay at the branching point, under which condition the two shock waves tend to merge into one, as shown in Fig. 6e. At this critical state, the critical backpressures of the inner channel and the outer channel are 0.62 and 0.34 MPa, which account for 88.6 and 48.8% of the inlet total pressure, respectively. This means the critical backpressure of the inner channel is much higher than that of the outer channel at this point. There are two reasons for it. First, the fluid adjacent to the wall is the main stream of the source fluid in the outer channel, and a large part of the mechanical energy of the fluid adjacent to the wall transforms into heat due to strong friction, which causes lower total pressure in the outer channel. Second, obvious flow separation is observed in the outer channel, which also results in a great total pressure loss. If the two backpressures continue to increase, it can be inferred that the merged shock wave continues to move to the upstream of the branching point, as shown in Fig. 6d. However, if one of the backpressures is lower than the critical value and the other is higher than that, the situations as presented in Figs. 6b and 6c occur. A shock wave exists in front of the branching point in the main channel, and the supersonic flow changes into a subsonic one after the shock. In the branching channel with higher backpressure, the gas flow maintains its subsonic speed. On the contrary, in the branching channel with lower backpressure, the flow reaccelerates to be

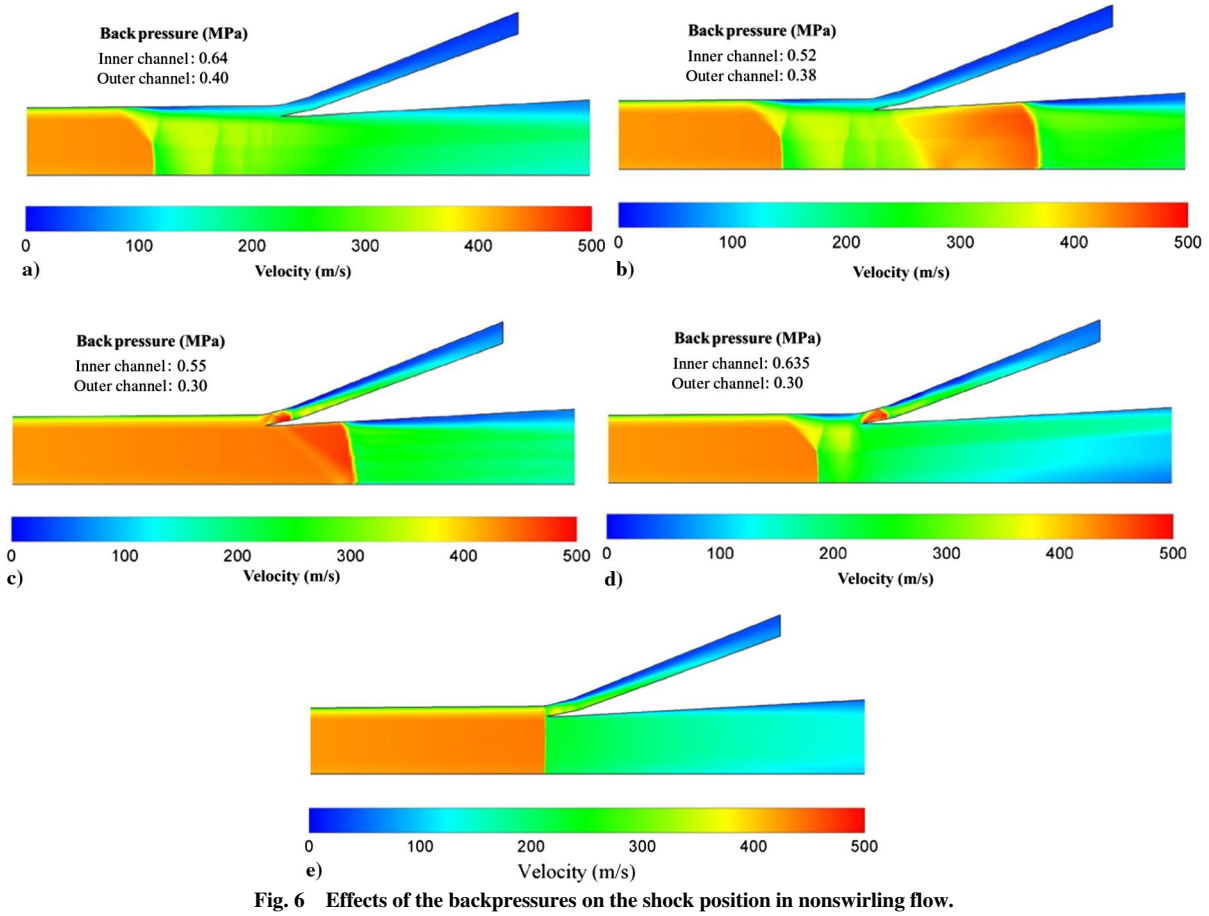

Fig. 6 Effects of the backpressures on the shock position in nonswirling flow.

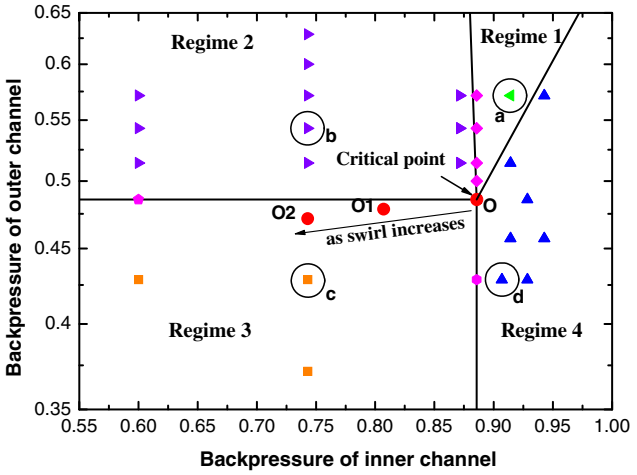

Fig. 7 Four flow regimes in supersonic branching flow.

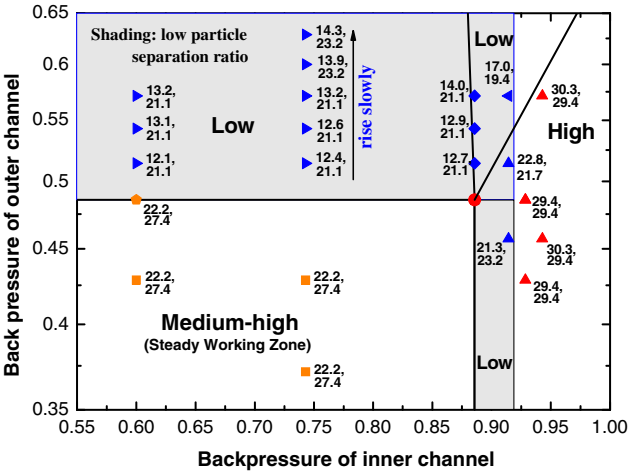

Fig. 8 Gas flow ratio and particle separation ratio.

supersonic and another shock wave emerges (see the outer channel in Fig. 6b and the inner channel in Fig. 6c).

Based on the aforementioned analysis, we conclude that there are four flow regimes in the supersonic branching flow in terms of the shock wave position(s), namely 1) shock in the main channel, 2) shock in the main channel and the inner branch, 3) shock in both of the branches, and 4) shock in the main channel and the outer branch. And, these four regimes are schematically shown in Fig. 7. The backpressures are nondimensionalized by being divided by the inlet pressure of 0.7 MPa. The symbols in the figure represent the study cases, and the study cases in Figs. 6a, 6b, 6c, and 4d are demonstrated in Fig. 7 as a, b, c, and d, respectively. The critical point in Fig. 7 represents the critical state mentioned previously. It is notable that, unlike the borders between 1 and 2, 2 and 3, and 3 and 4, the border between 1 and 4 is neither horizontal nor vertical. This is because the backpressure of the inlet channel is so high that a larger part of the gas flow is forced to go through the outer channel, which results in the reacceleration of the flow and the emergence of the shock wave in the outer channel. The division of the borders is determined by various factors such as the geometry of the branching tube and the working conditions, which can seriously affect the interaction between the flows in the inner branch and in the outer branch.

B. Gas Flow Rate Ratio and Particle Separation Ratio

The flow and particle distribution between the two branches in supersonic branching flow is our main research concern. The gas flow rate ratio is defined as the ratio of the gas flow rate in the outer channel to the total flow rate, and the particle separation ratio is defined in a similar way, except that the gas flow rate is replaced by the particle flow rate.

Figure 8 shows the two ratios for the cases we have studied in the flow regime scheme. In Fig. 8, next to each symbol there are two numbers. The upper one indicates the gas flow rate ratio, and the lower one the particle separation ratio. Our careful examination of the two ratios for each case leads to the conclusion that they are related. Generally speaking, when the gas flow rate ratio rises, the particle separation ratio rises. This conclusion can be further justified by the fact that the particle in our study here is 1.0 μm in diameter and 1000 kg/m^3 in density, and it shows a strong tendency to follow the gas phase.

According to the value of the particle separation ratio, the space in Fig. 8 can be divided into three regions, namely, the medium-high region, the low region, and the high region. In the medium-high region, identical values of the particle separation ration result for all the cases. This medium-high region coincides with regime 3 in Fig. 7. In this regime, the shock waves occur in the two branches and the flow in the main channel is supersonic. Thus, an undisturbed state is formed in the main channel and, at this state, the flow and particle separation in the main channel is free from the effects of the changing backpressures. Therefore, in terms of the main channel, we define this region as the steady working zone.

If either of the backpressures rises and pushes the shock wave upstream into the main channel (i.e., the transition from regime 3 to regime 2 or 4), a sudden drop of the two ratios occurs. The reason lies in the shock wave/boundary-layer interaction, as shown in Fig. 9. According to the principles of the shock wave/boundary-layer interaction, flow separation occurs behind the shock wave in the boundary layer. In Fig. 6, the separation due to the shock/boundary-layer interaction is obvious. The boundary layer in the main channel is about one-fifth of the radius, so the separation changes the downstream flow after the shock wave to a large extent. Once the separation occurs, the gas flow ratio decreases rapidly, which is because the boundary-layer separation causes lower flow rate in the outer branch. Consequently, fewer particles enter the outer branch. Figure 4 also shows the change of the average particle trajectory caused by the shock wave/boundary-layer interaction. In this figure, the particle suddenly moves away from the wall at $t \approx 0.23$ ms, indicating the occurrence of the flow separation. It also can be noticed that, in regime 2, the two ratios change little as the backpressure of the inner channel increases, which is because, in this case, the shock wave migration in the outer channel does not affect the flow so much as in the main channel.

If either of the backpressures continues to increase, the shock wave in the main channel keeps moving upstream and, in this case, there are two outcomes for the shock wave/boundary-layer interaction. The first is that this interaction becomes less obvious due to the decrease of the shock intensity. The second is the flow gets the time to reattach before reaching the branching point. As a result, the gas flow ratio and the particle separation ratio start rising again, as designated by arrows in Fig. 8. They rise slowly in the vertical direction but rapidly in the horizontal direction. That is because the shock in the main channel is more sensitive to the changing backpressure of the inner channel, i.e., when backpressure of the inner channel increases, the shock wave moves upstream rapidly. But, it moves slowly when the backpressure of the outer channel increases. In fact, in a de Laval nozzle the ratio of the backpressure to the total pressure represents the motive energy for the flow and determines the maximum Mach number the flow can

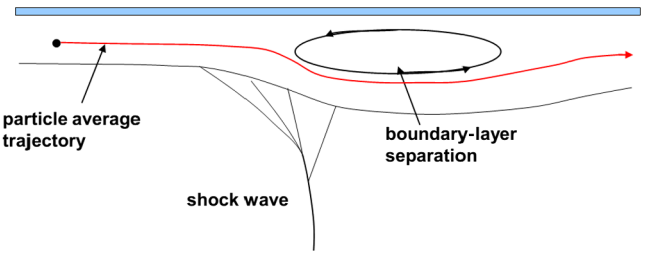

Fig. 9 Effect of the shock/boundary-layer interaction on the particle motion.

reach. Similarly, in supersonic branching flow, there are two energy sources. Apparently, the backpressure of the inner channel is the more dominating one because the larger part of the flow goes through the inner channel. Thus, a change in the backpressure of the inner channel causes a stronger reaction of the shock wave in the main channel. Besides, as mentioned previously, the critical pressures of the inner channel and that of the outer channel are 88.6 and 48.8% of the inlet total pressure, respectively. And, it means there is little room for the backpressure of the inner channel, but relatively much room for the backpressure of the outer channel to raise its percentage of the inlet total pressure to 100%, which is also the reason why the shock wave is more sensitive to the changing backpressure of the inner channel. To sum up, in regimes 1, 2, and 4, the flowfield in the main channel is disturbed by the flow conditions in the branches downstream, resulting in a change in the two ratios as the backpressures vary. So, the region these three regimes cover is defined as the disturbed working zone.

C. Effects of the Swirl

To examine the effect of the swirl on the particle motion, the supersonic swirling flow is investigated. The swirl is introduced from the inlet with the same tangential velocity in the radial direction, i.e., $V_{in\theta}/V_{inx}$. As the average radius of the accelerating annular channel decreases, the average swirling velocity increases dramatically. Generally, it develops into a Rankine vortex flow in the main channel, as shown in Fig. 10.

There are two effects the swirl brings to the branching flow. First, the total friction between the gas and the wall increases a little. Second, vortex breakdown emerges behind the shock wave. Vortex breakdown is characterized by a sudden change in the vortex structure [25]. Usually, recirculation zones or spirals emerge when it happens [26–28]. The axisymmetric formulation can be used to obtain useful results of the vortex breakdown [15]. In our study, the vortex breakdown is observed in Fig. 10, where the swirling intensity suddenly falls near the branching point, especially in the vicinity of the axis. Also, Fig. 11 shows that the vortex breakdown happens downstream of the shock wave. In Figs. 11b and 11c, it emerges right behind the shock wave. In fact, in our study, the flow with vortex breakdown is unsteady and oscillating. Nevertheless, the unsteadiness is mainly in the vortex breakdown zone and the position of the shock wave is almost unaffected. The vortex breakdown can be either beneficial or hazardous for practical applications. For example, it helps to keep combustion flames stable in swirling flow [29], but the lift force on a delta wing decreases when it happens [30].

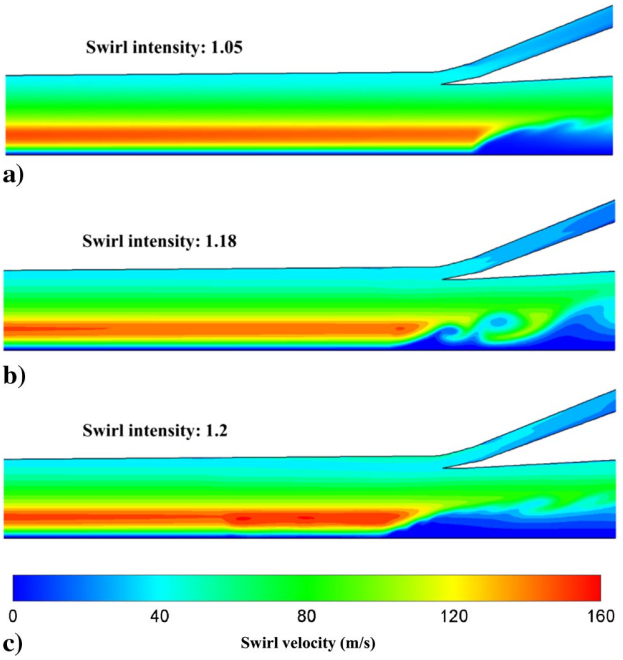

Fig. 10 Swirl velocity contour near the branching point at different swirl intensities.

In our study case, the raise of the total pressure loss caused by the vortex breakdown is considerable but that contributed by the friction increase is little, which brings about two consequences for the branching flow as the swirl increases. The first one is that the shock wave moves upstream when the two backpressures keep constant, as shown in Fig. 11. This is predictable when the motive energy is consumed faster. The second one is that, in the flow regime map, there is a drift of the critical state (see Fig. 7). Both of the critical pressures decrease as the swirl increases. However, the critical backpressure of the inner channel falls much faster than that of the outer channel. That is because the pressure loss in the outer channel is primarily caused by the friction and that in the inner channel is mainly due to the vortex breakdown.

D. Effects of Particle Size

It is easily inferred that the particle with larger size moves toward the wall more quickly than the one with smaller size in swirling flows. In fact, as the mass of a particle is proportional to the cubic square of its diameter, the particle's radial velocity depends on the particle size, as shown in Fig. 12. In this figure, the effect of the shock wave/boundary-layer interaction is eliminated by displacing the shock wave from the main channel. Also, it turns out that the larger particle does not show a different reaction to the shock wave/boundary-layer interaction in the absence of swirl. Figure 12 shows that the separation efficiency is almost constant when the particle size varies from 0.05 to 3.0 μm and the swirl is set zero. The reason is that the Stokes number for 1 μm particles in the main flow is around 0.2, which is far below one. So, we can see that the particles have a strong tendency to flow the gas.

VI. Discussion

The discussion section focuses on the steady working zone (regime 3) in the main channel, which has practical significance for industrial applications. In fact, once the critical backpressures are given, the range of the steady working zone is then determined. However, the critical backpressures are influenced by multiple factors, including the intensity of the shock wave, friction, separation of the boundary layer, and even the vortex breakdown. The main purpose of the discussion part is to provide a convenient way to estimate the gas flow rate ratio in two simplified ideal cases.

A. Nonswirling Flow Without Friction

In nonswirling supersonic branching flow, if the branching flow channel is large enough and the friction in the channel is neglected, the expansion before the shock wave and the compression after the shock wave can be assumed as isentropic. Once the structure is established and the ratio of the backpressure to the total pressure is determined, the critical state for this structure is determined. In this case, the critical backpressures can be obtained by calculating the total pressure loss due to the shock wave, and the gas flow rate ratio for the steady working zone is determined exclusively by the ratio of the outer channel cross-sectional area to the total cross-sectional area at the branching point: $\eta = \dot{m}_{out}/\dot{m}_{total} = A_{out}/A_{total}$. It is worthy of note that this inference is only valid for the nonswirling, frictionless, perfect gas flow of certain working fluids.

B. Nonswirling Flow with Friction

Under some circumstances, friction cannot be neglected, and it even plays an important role, like the case in this research. For the viscous fluid, separation of the boundary layer occurs due to the shock wave/boundary-layer separation, and our following discussion does not include the analysis on the critical backpressures under such conditions. We focus on the gas flow rate ratio for the steady working zone.

The friction of the wall causes a decrease in the velocity and an expansion of the gas adjacent to the wall that, in consequence, lowers the gas flow rate in the outer channel. In most cases, the thickness of

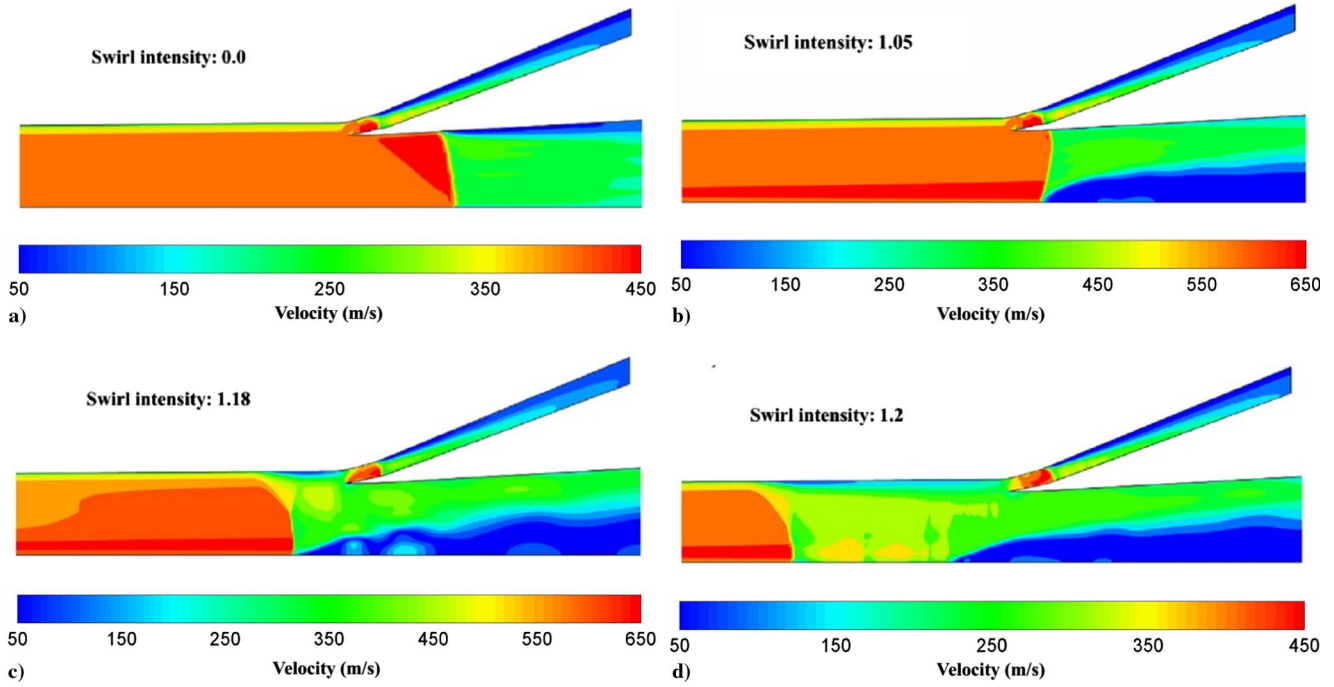

Fig. 11 Effects of the swirl intensity on the shock position.

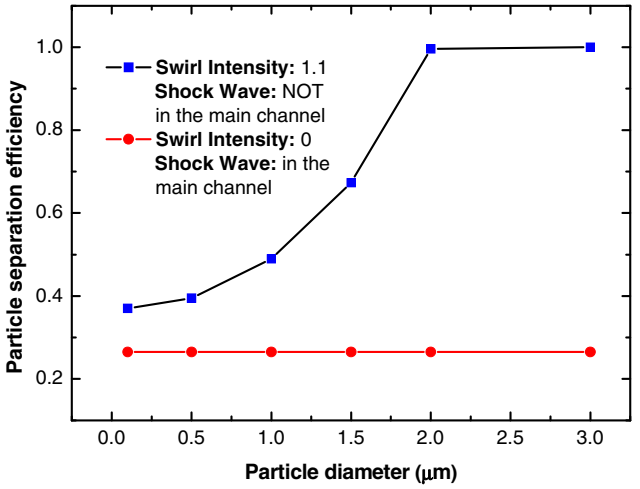

Fig. 12 Effects of the particle diameter on separation efficiency.

the boundary layer is less than the width of the outer channel. The actual gas flow rate ratio in the presence of friction can be estimated with

$$\eta = \frac{\dot{m}_{\text{out}}}{\dot{m}_{\text{total}}} = \frac{\dot{m}'_{\text{out}} - \Delta\dot{m}}{\dot{m}'_{\text{total}} - \Delta\dot{m}} \tag{6}$$

where $\dot{m}_{\text{out}}$ and $\dot{m}_{\text{total}}$ are the actual gas flow rate in the outer channel and the total gas flow rate, respectively. The gas flow rate in the outer channel and the total gas flow rate in the absence of friction are $\dot{m}'_{\text{out}}$ and $\dot{m}'_{\text{total}}$, respectively. $\Delta\dot{m}$ is the decrease of the gas flow rate when friction is taken into account. Although $\dot{m}'_{\text{out}}$ and $\dot{m}'_{\text{total}}$ can be readily obtained, $\Delta\dot{m}$ is more complex.

The key to the expression of $\Delta\dot{m}$ is the displacement thickness of the boundary layer δ^*:

$$\Delta\dot{m} = \rho_B V_B C_B \delta^* \tag{7}$$

where ρ_B and V_B are the density and velocity of the fluid at the outer edge of the boundary layer at branching point B, respectively. C_B is the circumference of the main channel at branching point B. We can get the expression of δ^* as

$$\delta^* = \int_0^\delta \left\{ 1 - \frac{(y/\delta)^{1/n}}{1 + (V_\infty^2/2c_pT_\infty)[1 - (y/\delta)^{2/n}]} \right\} \mathrm{d}y \tag{8}$$

V_∞, ρ_∞, and T_∞ are the velocity, density, and temperature at the outer edge of the boundary layer at branching point B, respectively; and $n = 2.2Re_x^{1/14}(1 + 0.2M)^{1/7}$ [31]. The effective radius at point B is $R_B - \delta^*$, where R_B is the real radius of the main channel at point B. Also, δ can be obtained analytically, experimentally or from numerical simulation. Then, δ^* can be calculated with a numerical quadrature like the Newton–Cotes formulas.

For the geometrical structure and the conditions in this research, we analyze the actual gas flow rate ratio by following the aforementioned procedures. For example, the boundary-layer thickness in our case is 0.85 mm at the branching point. Then, the actual gas flow rate ratio we obtain is 22.97%. Compared with the result from numerical simulations (that is, 22.2%), our result has a relative error of 3.47%. If friction is neglected, the gas flow rate ratio of 28.76% is equal to the ratio of the outer channel cross-sectional area to the total cross-sectional area at the branching point, and it is much higher than the real one.

VII. Conclusions

In this paper, the particle-laden supersonic branching flow is simulated with the Eulerian–Lagrangian method. The model used is a two-dimensional axisymmetric one with a pointwise approach for particles. Although the three-dimensional structures in the vortex breakdown zone cannot be accurately simulated, the key features of the supersonic branching flow are revealed in this research. It is found that there are four flow regimes in terms of the shock wave position in supersonic branching flow, namely, 1) shock in the main channel, 2) shock in the main channel and the inner branch, 3) shock in both branches, and 4) shock in the main channel and the outer branch. And, the gas flow ratio and the particle separation ratio are closely related to these four regimes. The steady working zone exists in terms of the flow in the main channel, in which the gas flow rate ratio and particle separation ratio are not affected by the backpressures. As the particle is small, and thus follows the gas phase well in the absence of swirl, the particle separation ratio and the gas flow ratio show a similar trend. If there is a swirl in the flow, the critical state for the four regimes drifts on the regime map in the direction of the falling backpressures, which is caused by the increasing total pressure loss

due to the vortex breakdown and rising friction. The effects of the particle size are also studied. The effects of the flow separation induced by the shock wave on the particle motion are not sensitive to the change of the particle size. However, the particle separation ratio does increase rapidly in swirling flow if the particle is larger. The gas flow rate ratio for the steady working zone with and without considering friction is discussed. In the current study cases, friction is influential and causes a dramatic decrease of the ratio.

It is necessary to point out that the current regime map is true only for the channel of the present geometrical structure of the branching flow and the working conditions in the current research. Under different conditions, the regime map can be different. For example, in swirling flow, factors like the geometry of the channel, total pressure, or gas properties may affect the regime map, including the critical state drift and the borders between regimes. Also, if the geometrical structure is large enough, the boundary-layer separation may not influence the flowfield as remarkably as it does in the current research. For all these uncertainties, one thing for sure about supersonic branching flow is the four regimes. Therefore, a preliminary research into this kind of flow becomes a reality and provides a foundation for further research.

Acknowledgments

This work was financially supported by the China National Funds for Distinguished Young Scientists under contract no. 51425603 and the Open Project of State Key Laboratory of Multiphase Flow in Power Engineering.

References

[1] Brooke, J. W., Kontomaris, K., Hanratty, T. J., and Mclaughlin, J. B., "Turbulent Deposition and Trapping of Aerosols at a Wall," *Physics of Fluids A — Fluid Dynamics*, Vol. 4, No. 4, 1992, pp. 825–834. doi:10.1063/1.858299

[2] Lyons, S. L., Hanratty, T. J., and Mclaughlin, J. B., "Large-Scale Computer-Simulation of Fully-Developed Turbulent Channel Flow with Heat-Transfer," *International Journal for Numerical Methods in Fluids*, Vol. 13, No. 8, 1991, pp. 999–1028. doi:10.1002/fld.1650130805

[3] Marchioli, C., and Soldati, A., "Mechanisms for Particle Transfer and Segregation in a Turbulent Boundary Layer," *Journal of Fluid Mechanics*, Vol. 468, Oct. 2002, pp. 283–315. doi:10.1017/S0022112002001738

[4] Mclaughlin, J. B., "Aerosol-Particle Deposition in Numerically Simulated Channel Flow," *Physics of Fluids A — Fluid Dynamics*, Vol. 1, No. 7, 1989, pp. 1211–1224. doi:10.1063/1.857344

[5] Soldati, A., and Marchioli, C., "Physics and Modelling of Turbulent Particle Deposition and Entrainment: Review of a Systematic Study," *International Journal of Multiphase Flow*, Vol. 35, No. 9, 2009, pp. 827–839. doi:10.1016/j.ijmultiphaseflow.2009.02.016

[6] Theofanous, T. G., "Aerobreakup of Newtonian and Viscoelastic Liquids," *Annual Review of Fluid Mechanics*, Vol. 43, No. 1, 2011, pp. 661–690. doi:10.1146/annurev-fluid-122109-160638

[7] Meng, J. C., and Colonius, T., "Numerical Simulations of the Early Stages of High-Speed Droplet Breakup," *Shock Waves*, Vol. 25, No. 4, July 2015, pp. 399–414, doi:10.1007/s00193-014-0546-z

[8] Goossens, H. W. J., Cleijne, J. W., Smolders, H. J., and Vandongen, M. E. H., "Shock-Wave Induced Evaporation of Water Droplets in a Gas-Droplet Mixture," *Experiments in Fluids*, Vol. 6, No. 8, 1988, pp. 561–568. doi:10.1007/BF00196603

[9] Kersey, J., Loth, E., and Lankford, D., "Effects of Evaporating Droplets on Shock Waves," *AIAA Journal*, Vol. 48, No. 9, 2010, pp. 1975–1986. doi:10.2514/1.J050162

[10] Li, X., and Bai, B., "Motion of Submicron Particles in Supersonic Laminar Boundary Layers," *AIAA Journal*, Vol. 53, No. 4, 2015, pp. 1037–1047. doi:10.2514/1.J053364

[11] Bagchi, P., and Balachandar, S., "Inertial and Viscous Forces on a Rigid Sphere in Straining Flows at Moderate Reynolds Numbers," *Journal of Fluid Mechanics*, Vol. 481, April 2003, pp. 105–148. doi:10.1017/S002211200300380X

[12] Ling, Y., Haselbacher, A., and Balachandar, S., "Importance of Unsteady Contributions to Force and Heating for Particles in Compressible Flows: Part 1: Modeling and Analysis for Shock-Particle Interaction," *International Journal of Multiphase Flow*, Vol. 37, No. 9, 2011, pp. 1026–1044. doi:10.1016/j.ijmultiphaseflow.2011.07.001

[13] Balachandar, S., and Eaton, J. K., "Turbulent Dispersed Multiphase Flow," *Annual Review of Fluid Mechanics*, Vol. 42, No. 1, 2010, pp. 111–133. doi:10.1146/annurev.fluid.010908.165243

[14] Li, S. Q., Marshall, J. S., Liu, G. Q., and Yao, Q., "Adhesive Particulate Flow: The Discrete-Element Method and Its Application in Energy and Environmental Engineering," *Progress in Energy and Combustion Science*, Vol. 37, No. 6, 2011, pp. 633–668. doi:10.1016/j.pecs.2011.02.001

[15] Umeh, C. O. U., Rusak, Z., Gutmark, E., Villalva, R., and Cha, D. J., "Experimental and Computational Study of Nonreacting Vortex Breakdown in a Swirl-Stabilized Combustor," *AIAA Journal*, Vol. 48, No. 11, 2010, pp. 2576–2585. doi:10.2514/1.J050393

[16] Loth, E., "Compressibility and Rarefaction Effects on Drag of a Spherical Particle," *AIAA Journal*, Vol. 46, No. 9, 2008, pp. 2219–2228. doi:10.2514/1.28943

[17] Yamamoto, K., and Ishihara, Y., "Thermophoresis of a Spherical Particle in a Rarefied Gas of a Transition Regime," *Physics of Fluids*, Vol. 31, No. 12, 1988, Paper 3618. doi:10.1063/1.866878

[18] Saffman, P. G., "The Lift on a Small Sphere in a Slow Shear Flow," *Journal of Fluid Mechanics*, Vol. 22, No. 2, 1965, pp. 385–400. doi:10.1017/S0022112065000824

[19] Dandy, D. S., and Dwyer, H. A., "A Sphere in Shear Flow at Finite Reynolds Number: Effect of Shear on Particle Lift, Drag, and Heat Transfer," *Journal of Fluid Mechanics*, Vol. 216, July 1990, pp. 381–410. doi:10.1017/S0022112090000477

[20] McLaughlin, J. B., "The Lift on a Small Sphere in Wall-Bounded Linear Shear Flows," *Journal of Fluid Mechanics*, Vol. 246, Jan. 1993, pp. 249–249. doi:10.1017/S0022112093000114

[21] Mei, R., "An Approximate Expression for the Shear Lift Force on a Spherical Particle at Finite Reynolds Number," *International Journal of Multiphase Flow*, Vol. 18, No. 1, 1992, pp. 145–147. doi:10.1016/0301-9322(92)90012-6

[22] Kurose, R., and Komori, S., "Drag and Lift Forces on a Rotating Sphere in a Linear Shear Flow," *Journal of Fluid Mechanics*, Vol. 384, No. 4, 1999, pp. 183–206. doi:10.1017/S0022112099004164

[23] Bagchi, P., and Balachandar, S., "Effect of Free Rotation on the Motion of a Solid Sphere in Linear Shear Flow at Moderate Re," *Physics of Fluids*, Vol. 14, No. 8, 2002, pp. 2719–2737. doi:10.1063/1.1487378

[24] Tedeschi, G., Gouin, H., and Elena, M., "Motion of Tracer Particles in Supersonic Flows," *Experiments in Fluids*, Vol. 26, No. 4, 1999, pp. 288–296. doi:10.1007/s003480050291

[25] Leibovich, S., "The Structure of Vortex Breakdown," *Annual Review of Fluid Mechanics*, Vol. 10, No. 1, 1978, pp. 221–246. doi:10.1146/annurev.fl.10.010178.001253

[26] Sørensen, J. N., Naumov, I. V., and Okulov, V. L., "Multiple Helical Modes of Vortex Breakdown," *Journal of Fluid Mechanics*, Vol. 683, Sept. 2011, pp. 430–441. doi:10.1017/jfm.2011.30

[27] Oberleithner, K., Paschereit, C. O., Seele, R., and Wygnanski, I., "Formation of Turbulent Vortex Breakdown: Intermittency, Criticality, and Global Instability," *AIAA Journal*, Vol. 50, No. 7, 2012, pp. 1437–1452. doi:10.2514/1.J050642

[28] Malalasekera, W., Ranga-Dinesh, K. K. J., Ibrahim, S. S., and Masri, A. R., "LES of Recirculation and Vortex Breakdown in Swirling Flames," *Combustion Science and Technology*, Vol. 180, No. 5, 2008, pp. 809–832. doi:10.1080/00102200801894018

[29] Syred, N., and Beér, J. M., "Combustion in Swirling Flows: A Review," *Combustion and Flame*, Vol. 23, No. 2, 1974, pp. 143–201. doi:10.1016/0010-2180(74)90057-1

[30] Spall, R. E., Gatski, T. B., and Grosch, C. E., "A Criterion for Vortex Breakdown," *Physics of Fluids*, Vol. 30, No. 11, 1987, pp. 3434–3440. doi:10.1063/1.866475

[31] Schlichting, H., *Boundary-Layer Theory*, 7th ed., McGraw–Hill, New York, 1979, Chaps. XIII, XXIII.

R. P. Lucht
Associate Editor